J|A|C|S
ARTICLES

Published on Web 04/08/2009

Unusual Luminescence Enhancement of Metallogels of Alkynylplatinum(II) 2,6-Bis(*N*-alkylbenzimidazol-2′-yl)pyridine Complexes upon a Gel-to-Sol Phase Transition at Elevated Temperatures

Anthony Yiu-Yan Tam, Keith Man-Chung Wong, and Vivian Wing-Wah Yam*

Centre for Carbon-Rich Molecular and Nano-Scale Metal-Based Materials Research, Department of Chemistry, and HKU-CAS Joint Laboratory on New Materials, The University of Hong Kong, Pokfulam Road, Hong Kong

Received February 10, 2009; E-mail: wwyam@hku.hk

Abstract: A series of alkynylplatinum(II) complexes of 2,6-bis(*N*-alkylbenzimidazol-2′-yl)pyridine has been synthesized and characterized by ^{1}H NMR, IR, FAB mass spectrometry, and elemental analysis; the photophysical properties have also been investigated. All the complexes have been shown to exhibit interesting gelation properties. Scanning electron microscopy (SEM) of the xerogels showed a network of fibrous structures, typical of morphologies of organogels/metallogels. Interestingly, two of the complexes were found to show strong luminescence enhancement upon a gel-to-sol phase transition upon increasing the temperature. This unusual behavior is rarely encountered, as it represents a sharp contrast to that exhibited by other typical thermotropic organogels and metallogels reported so far. Variable-temperature UV−vis and luminescence spectroscopies were performed to probe the gel-to-sol phase transition. Concentration-dependent, variable-temperature, and time-resolved emission studies in dilute benzene solution have also been made to provide further insights into the spectroscopic origin in the sol forms. A quantitative treatment of the system based on the Birks scheme has been performed.

Introduction

Supramolecular chemistry constitutes a branch of science that is of growing importance owing to its numerous implications upon materials and biological applications. This field pertains to the study of weak non-covalent interactions,[1] with most studies confined to organic systems with hydrogen-bonding, hydrophobic−hydrophobic, and $\pi-\pi$ interactions. Only in the past two decades has there been a revival of interest in the study of metal complexes with metal−metal interactions, particularly in the area of low-dimensional gold(I)[2] and platinum(II)[3−5] chemistry. A proper understanding of the underlying non-covalent interactions that govern supramolecular assemblies and determine the different hierarchies of organization going from molecules to devices or molecules to biological assemblies is particularly important, as these interactions would in turn govern the properties and performance of the materials and biological processes. In the past decade, low-molecular-weight organogels, in particular, have attracted much attention.[6] Their attractiveness over traditional polymers, which utilize covalent interactions to construct a giant molecule from smaller molecules, lies in the provision of a "bottom-up" approach to the design and synthesis of functional materials on nano- or micrometer scales through non-covalent interactions.[1b] These weak non-covalent

(1) (a) Lehn, J.-M. *Comprehensive Supramolecular Chemistry*; Pergamon Press: Oxford, UK, 1996. (b) Goodby, J. W.; Saez, I. M.; Cowling, S. J.; Görtz, V.; Draper, M.; Hall, A. W.; Sia, S.; Cosquer, C.; Lee, S. E.; Raynes, E. P. *Angew. Chem., Int. Ed.* **2008**, *47*, 2.

(2) (a) Assefa, Z.; McBurnett, B. G.; Staples, R. J.; Fackler, J. P., Jr.; Assmann, B.; Angermaler, K.; Schmidbaur, H. *Inorg. Chem.* **1995**, *34*, 7. (b) Forward, J. M.; Bohmann, D.; Fackler, J. P., Jr.; Staples, R. J. *Inorg. Chem.* **1995**, *34*, 6330. (c) Wilton-Ely, J. D. E. T.; Schier, A.; Schmidbaur, H. *Organometallics* **2001**, *20*, 1895.

(3) (a) Yam, V. W. W.; Tang, R. P. L.; Wong, K. M. C.; Cheung, K. K. *Organometallics* **2001**, *20*, 4476. (b) Yam, V. W. W.; Wong, K. M. C.; Zhu, N. *J. Am. Chem. Soc.* **2002**, *124*, 6506. (c) Yam, V. W. W.; Chan, K. H. Y.; Wong, K. M. C.; Chu, B. W. K. *Angew. Chem., Int. Ed.* **2006**, *45*, 6169. (d) Yu, C.; Wong, K. M. C.; Chan, K. H. Y.; Yam, V. W. W. *Angew. Chem., Int. Ed.* **2005**, *44*, 791. (e) Yu, C.; Chan, K. H. Y.; Wong, K. M. C.; Yam, V. W. W. *Proc. Natl. Acad. Sci. U.S.A.* **2006**, *103*, 19652. (f) Yam, V. W. W.; Chan, K. H. Y.; Wong, K. M. C.; Zhu, N. *Chem.—Eur. J.* **2005**, *11*, 4535. (g) Tam, A. Y. Y.; Wong, K. M. C.; Wang, G.; Yam, V. W. W. *Chem. Commun.* **2007**, 2028.

(4) (a) Eryazici, I.; Moorefield, C. N.; Newkome, G. R. *Chem. Rev.* **2008**, *108*, 1834. (b) Camerel, F.; Ziessel, R.; Donnio, B.; Bourgogne, C.; Guillon, D.; Schmutz, M.; Iacovita, C.; Bucher, J. P. *Angew. Chem., Int. Ed.* **2007**, *46*, 2659. (c) Yip, H. K.; Cheng, L. K.; Cheung, K. K.; Che, C. M. *J. Chem. Soc., Dalton Trans.* **1993**, 2933. (d) Bailey, J. A.; Hill, M. G.; Marsh, R. E.; Miskowski, V. M.; Schaefer, W. P.; Gray, H. B. *Inorg. Chem.* **1995**, *34*, 4591. (e) Wadas, T. J.; Wang, Q.-M.; Kim, Y.-J.; Flaschenreim, C.; Blanton, T. N.; Eisenberg, R. *J. Am. Chem. Soc.* **2004**, *126*, 16841.

(5) (a) Wang, K.-Z.; Haga, M. A.; Monjushiro, H.; Akiba, M.; Sasaki, Y. *Inorg. Chem.* **2000**, *39*, 4022. (b) Grove, L. J.; Rennekamp, J. M.; Jude, H.; Connick, W. B. *J. Am. Chem. Soc.* **2004**, *126*, 1594.

(6) (a) Abdallah, D. J.; Weiss, R. G. *Adv. Mater.* **2000**, *12*, 1237. (b) Ishi-I, T.; Shinkai, S. *Top. Curr. Chem.* **2005**, *258*, 119. (c) Wang, C.; Zhang, D.; Xiang, J.; Zhu, D. *Langmuir* **2007**, *23*, 9195. (d) Bao, C.; Lu, R.; Jin, M.; Xue, P.; Tan, C.; Liu, G.; Zhao, Y. *Org. Biomol. Chem.* **2005**, *3*, 2508. (e) An, B. K.; Lee, D. S.; Lee, J. S.; Park, Y. S.; Song, H. S.; Park, S. Y. *J. Am. Chem. Soc.* **2004**, *126*, 10232. (f) Kamikawa, Y.; Kato, T. *Langmuir* **2007**, *23*, 274. (g) Jung, J. H.; Shinkai, S.; Shimizu, T. *Chem. Record* **2003**, *3*, 212. (h) Kamikawa, Y.; Kato, T. *Langmuir* **2007**, *23*, 274. (i) Camerel, F.; Bonardi, L.; Schmutz, M.; Ziessel, R. *J. Am. Chem. Soc.* **2006**, *128*, 11663. (j) Qu, Songnan; Zhao, L.; Yu, Z.; Xiu, Z.; Zhao, C.; Zhang, P.; Long, B.; Li, M. *Langmuir* **2009**, *25*, 1713.

interactions could further be readily weakened or even destroyed upon exposure to external stimuli, such as heat, and provide a versatile means for the controlled design of stimuli-responsive functional materials. There has also been an increasing interest in the use of coordination and organometallic compounds for the formation of metallogels since some of them showed rich spectroscopic and luminescence properties,[3g,4b,7a−e] as well as catalytic properties.[7f−i]

Luminescent square-planar d^8 platinum(II) terpyridyl complexes belong to one class of coordination compounds that has attracted much attention due to their intriguing spectroscopic and luminescence properties,[3,4,7a,8] as well as their propensity to exhibit metal−metal and $\pi-\pi$ interactions.[3,4] Among them, the organometallic alkynylplatinum(II) terpyridyl complexes have been found to show drastic color changes and luminescence enhancement due to the intermolecular aggregation and oligomerization induced by microenvironmental changes and external stimuli, such as changes in temperature[3c,g,4b] and solvent composition,[3b,f] or addition of polymers[3d] and biomolecules.[3e]

Recent efforts by us and others also demonstrated that alkynylplatinum(II) terpyridyl complexes showed drastic color changes during the sol−gel phase transition.[3g,4b] Similar to the other types of organogels and metallogels,[6c,h−j,7d] a decrease in the luminescence quantum yield in the sol form at higher temperature relative to the gel form was observed in these systems and was rationalized by the fluidity of the sol form and the more facile non-radiative decay that occurs at higher temperature.[3g] For the same reasons, it has generally been widely accepted that most other materials and solutions usually show a lower luminescence quantum yield with increasing temperature.

Apart from the development of platinum(II) terpyridyl complexes, platinum(II) complexes of other tridentate *N*-donor ligands, such as 2,6-bis(*N*-alkylbenzimidazol-2′-yl)pyridine (bzimpy),[5,9] have been explored by Haga and co-workers, who reported a lipophilic chloroplatinum(II) bzimpy complex that showed stable LB film-forming behavior and strong emission from the LB monolayer film.[5a] In contrast to its terpyridyl counterpart, the bzimpy ligand could readily be functionalized at the nitrogen atom of the benzimidazole group[5a,9] and the 4-position of the pyridine ring.[9]

Recently, our group reported the synthesis and isolation of a new series of alkynylplatinum(II) complexes of bzimpy ligand type.[9] The introduction of alkynyl groups was reported to enhance the luminescence properties. It is anticipated that the alkynylplatinum(II) complexes with the bzimpy functionalized with hydrophobic groups such as long alkyl chains are able to achieve gelation properties, forming stable metallogels in organic solvents through hydrophobic−hydrophobic interactions with incorporation of simple types of alkynyl ligands. Herein we report the synthesis and photophysical properties of the alkynylplatinum(II) bzimpy complexes (Scheme 1) as well as the study of their gelation properties. In sharp contrast to the typical behavior of thermotropic organogels and metallogels,[3g,6c,h−j,7d] which showed luminescence enhancement during gel formation, metallogels of **1** and **3** showed unusual luminescence enhancement during the gel-to-sol phase transition at elevated temperature.

Scheme 1. Structures of the Alkynylplatinum(II) bzimpy Complexes, **1**, **2**, and **3**

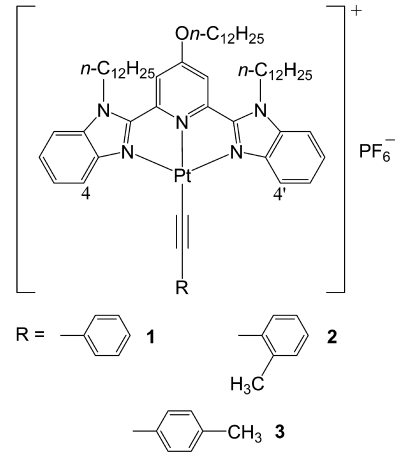

Results and Discussion

The alkynylplatinum(II) bzimpy complexes were synthesized by the reaction of the chloroplatinum(II) precursors with the corresponding alkynes in the presence of a catalytic amount of copper(I) iodide and triethylamine in dichloromethane solution. The identities of the platinum(II) complexes have been confirmed by ^{1}H NMR spectroscopy, FAB mass spectrometry, IR spectroscopy, and satisfactory elemental analyses. The IR spectra of **1**−**3** show a weak band at *ca.* 2114 cm^{-1}, typical of the ν(C≡C) stretching frequency.

The electronic absorption spectra of the complexes in dichloromethane solution at 298 K showed intense absorption bands at *ca.* 330−365 nm and less intense absorption bands or shoulders at *ca.* 440−446 nm. The photophysical data are summarized in Table 1. The high-energy intense absorption bands are assigned as intraligand (IL) [$\pi\rightarrow\pi^*$] transitions of the alkynyl and bzimpy ligands, while the low-energy less intense absorptions are tentatively assigned as an admixture of metal-to-ligand charge transfer (MLCT) [dπ(Pt)$\rightarrow\pi^*$(bzimpy)] and alkynyl-to-bzimpy ligand-to-ligand charge transfer (LLCT) [π(C≡C)$\rightarrow\pi^*$(bzimpy)] transitions.[9] The charge transfer (CT) assignment is consistent with the observation that **1** (λ = 440 nm) shows a higher-energy CT transition than **2** and **3** (λ = 465−466 nm), which can be rationalized by the presence of the electron-donating methyl substituents on the phenyl ring of the alkynyl ligand in **2** and **3** that would raise the dπ(Pt) and π(C≡C) orbital energies, leading to a lowering of the CT energy.[9]

All the complexes showed emissive properties in the solid state at 298 and 77 K and in butyronitrile glass at 77 K. Upon excitation at λ > 430 nm in dilute dichloromethane solutions (2×10^{-5} M) at 298 K, **1** showed vibronic-structured emission bands at 560 nm with vibrational progressional spacings of *ca.* 1300 cm^{-1}, while a structureless emission band at 610 nm was

(7) (a) Lu, W.; Law, Y. C.; Han, J.; Chui, S. S. Y.; Ma, D. L.; Zhu, N.; Che, C. M. *Chem. Asian J.* **2008**, *3*, 59. (b) Kishimura, A.; Yamashita, T.; Aida, T. *J. Am. Chem. Soc.* **2005**, *127*, 179. (c) Shirakawa, M.; Fujita, N.; Tani, T.; Kaneko, K.; Shinkai, S. *Chem. Commun.* **2005**, 4149. (d) Lam, S. T.; Wang, G.; Yam, V. W. W. *Organometallics* **2008**, *27*, 4545. (e) Fages, F. *Angew. Chem., Int. Ed.* **2006**, *45*, 1680. (f) Tu, T.; Assenmacher, W.; Peterlik, H.; Weisbarth, R.; Nieger, M.; Dötz, K. H. *Angew. Chem., Int. Ed.* **2007**, *46*, 6368. (g) Liu, Y.-R.; He, L.; Zhang, J.; Wang, X.; Su, C.-Y. *Chem. Mater.* **2009**, *21*, 557. (h) Xing, B.; Choi, M.-F.; Xu, B. *Chem.—Eur. J.* **2002**, *8*, 5028. (i) Miravet, J. F.; Escuder, B. *Chem. Commun.* **2005**, 5796.
(8) (a) Jennette, K. W.; Gill, J. T.; Sadownick, J. A.; Lippard, S. J. *J. Am. Chem. Soc.* **1976**, *98*, 6159. (b) Büchner, R.; Field, J. S.; Haines, R. J.; Cunningham, C. T.; McMillin, D. R. *Inorg. Chem.* **1997**, *36*, 6506. (c) McMillin, D. R.; Moore, J. J. *Coord. Chem. Rev.* **2002**, *229*, 113.
(9) Tam, A. Y. Y.; Lam, W. H.; Wong, K. M. C.; Zhu, N.; Yam, V. W. W. *Chem.—Eur. J.* **2008**, *14*, 4562.

Table 1. Photophysical Data for **1**−**3**

complex	medium (*T*/K)	absorption data λ_{max}/nm (ε/dm^3 mol^{-1} cm^{-1})	emission data λ_{em}/nm (τ_o/μs)
1	CH_2Cl_2 (298)	330 (36 040), 348 (33 545), 365 (29 275), 440 (4990)	[560, 605 (1.34)],[a] 670 (0.28)[b]
	C_6H_6 (338)	329 (19 700), 361 sh (14 320), 448 (3055)	[550, 592 (0.48)],[a] 650 (0.36)[c]
	solid (298)		640 (0.31)
	solid (77)		630 (3.32)
	glass[d] (77)		[530, 570 (6.44)],[a] 610 (3.68)[e]
2	CH_2Cl_2 (298)	330 (33 505), 350 (33 710), 365 (30 505), 465 sh (3330)	610 (0.38), 680 (0.22)[b]
	solid (298)		634 (0.95)
	solid (77)		610 (2.93)
	glass[d] (77)		[526, 566 (6.36)],[a] 605 (4.66)[e]
3	CH_2Cl_2 (298)	330 (25 705), 349 (24 575), 365 (21 915), 466 sh (3060)	610 (0.36), 680 (0.20)[b]
	solid (298)		635 (0.42)
	solid (77)		630 (3.42)
	glass[d] (77)		[535, 575 (8.40)],[a] 610 (4.02)[e]

[a] Vibronic-structured emission band. [b] Structureless emission band observed at concentration $\geq 10^{-3}$ M. [c] Structureless emission band observed at concentration $\geq 10^{-5}$ M. [d] In butyronitrile glass. [e] Structureless emission band observed at concentration $\geq 10^{-6}$ M.

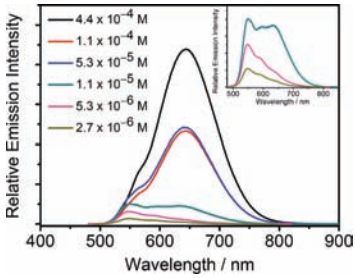

Figure 1. Corrected emission spectra of **1** in benzene solution at different concentrations at 338 K. Inset: Magnified emission spectra of **1** in benzene solution in the concentration range from 1.1×10^{-5} to 2.7×10^{-6} M at 338 K.

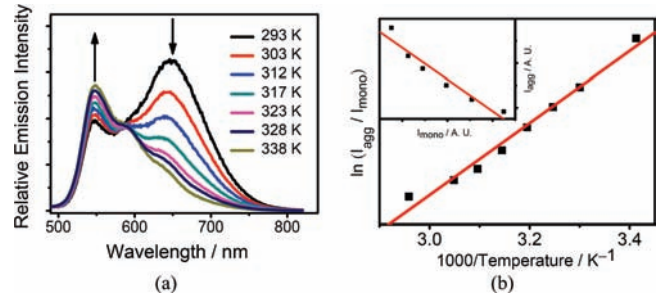

Figure 2. (a) Corrected emission spectra of **1** at different temperatures (increasing from 293 to 338 K) at concentration $= 2.7 \times 10^{-6}$ M and (b) the corresponding Stevens−Ban plot of $\ln(I_{agg}/I_{mono})$ vs $1/T$ (I_{agg} and I_{mono} are the emission intensities at 650 and 550 nm at corresponding temperatures). Inset: Corresponding plot of I_{agg} vs I_{mono}.

observed in **2** and **3**. With reference to previous spectroscopic work on the alkynylplatinum(II) bzimpy system,[9] the vibronic-structured emission band of **1** is derived from the metal-perturbed $\pi-\pi^*$ ^{3}IL excited state of the bzimpy ligand, while the structureless emission bands observed in **2** and **3** were derived from the triplet state of an admixture of MLCT and LLCT (^{3}MLCT/^{3}LLCT) origin. The difference in the luminescence behavior of **1** relative to **2** and **3** is ascribed to the subtle differences in the electron-donating properties of the alkynyl ligands.[9]

Interestingly, **1** showed concentration- and temperature-dependent emission properties in solution. Detailed concentration-dependent and variable-temperature UV−vis and luminescence spectroscopy and time-resolved emission spectroscopy of **1** were performed in benzene solutions. In very dilute solutions (2.7×10^{-6} M), **1** showed a vibronic-structured emission at 550 nm, similar to that observed in dilute dichloromethane solutions, while a structureless emission band was observed at 650 nm at high concentrations. Figure 1 shows the emission spectral changes of **1** with concentration. At concentrations decreasing from 4.4×10^{-4} to 2.7×10^{-6} M at 338 K, the low-energy structureless emission band at 650 nm was found to drop in intensity with a concomitant growth of a new vibronic-structured emission band at 550 nm. The most dilute sample ([**1**] $= 2.7 \times 10^{-6}$ M) was also subjected to variable-temperature luminescence study. On increasing the temperature of the dilute solution of **1** from 293 to 338 K, while no significant changes were observed in the variable-temperature UV−vis spectral traces, the low-energy broad emission band at 650 nm decreases in intensity while the high-energy vibronic-structured band at 550 nm increases in intensity upon excitation at $\lambda = 450$ nm, with a well-defined isoemissive point at 586 nm (Figure 2a). In view of the fact that the low-energy structureless emission band at 650 nm is both concentration- and temperature-dependent, an excimeric emission origin due to the formation of aggregate species in benzene solution is suggested, as it is well known that an increase in concentration or a lowering of temperature would favor aggregate formation.[10] Similarly, at concentrations $\geq 10^{-3}$ M and upon excitation at $\lambda = 480$ nm, new emission bands at *ca.* 670−680 nm were observed in dichloromethane solutions. This concentration-dependent structureless emission band was tentatively suggested to be derived from excimeric emission at high concentrations.[9] The variation of the ratio of aggregate or excimer to monomer intensities at various temperatures could be described by Birks kinetic scheme.[10] The Stevens−Ban plot of $\ln(I_{agg}/I_{mono})$ vs $1/T$ in benzene yields a positive slope (Figure 2b), indicative of the system being in the high-temperature limit (I_{agg} and I_{mono} are the emission intensities at 650 and 550 nm at the corresponding temperature, respectively).[10] Under this limit, an excimer binding enthalpy (ΔH) of -43.77 ± 2.49 kJ mol^{-1} has been obtained from the positive slope of the Stevens−Ban plot (Figure 2b) of a benzene solution of **1** (2.7×10^{-6} M).[10] A corresponding binding entropy (ΔS) of -44.14 J mol^{-1} K^{-1} has been obtained from the *y*-intercept of the Stevens−Ban plot and the negative slope of the plot of excimeric emission intensity at 650 nm against monomeric emission intensity at 550 nm (Figure 2b,

(10) (a) Birks, J. B. *Photophysics of Aromatic Molecules*; Wiley-Interscience: London, 1970. (b) Honda, C.; Katsumata, Y.; Yasutome, R.; Yamazaki, S.; Ishii, S.; Matsuoka, K.; Endo, K. *J. Photochem. Photobiol. A* **2006**, *18*, 151. (c) Aoudia, M.; Rodgers, M. A. J.; Wade, W. H. *J. Phys. Chem.* **1984**, *88*, 5008. (d) Halpern, A.; McBane, G. *Experimental Physical Chemistry*, 1st ed.; W. H. Freeman: New York, 2006.

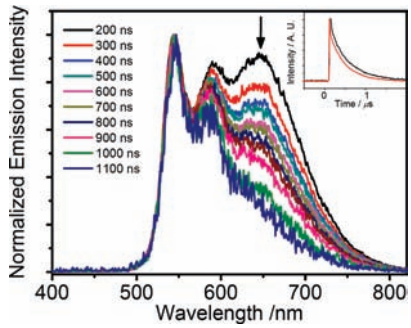

Figure 3. Normalized time-resolved emission spectra obtained at various gate delay from 200 to 1100 ns after the laser pulse for the benzene solution of **1** at 298 K ([Pt] = 3.9×10^{-6} M). Inset: Luminescence decay profiles of **1** in benzene solution monitored at 537 (black line) and 675 nm (red line).

inset).[10d] The Gibbs free energy change (ΔG) of the excimer formation and the monomer−excimer association constant at 298 K were calculated to be −30.62 kJ mol^{-1} and 2.33×10^5 M^{-1}, respectively. Time-resolved emission spectroscopy at various gate delay from 200 to 1100 ns was also performed in benzene solution of **1** ([**1**] = 3.9×10^{-6} M) at 298 K. At gate delay = 200 ns, both monomeric and excimeric emission bands were observed at 550 and 650 nm, respectively. Upon prolonging the gate delay from 200 to 1100 ns, the excimeric emission band disappeared, resulting from the faster decay of the excimeric excited state than that of the monomeric excited state at 298 K (Figure 3). The inset of Figure 3 shows the luminescence decay profiles of the emission bands at 537 and 675 nm, corresponding to the monomeric and excimeric emission bands, respectively. It shows that the monomeric excited state (0.48 μs) has a longer lifetime than the excimeric excited state (0.36 μs). Attempts to follow the kinetic correlation between the decay and rise profiles of the monomer and excimer bands, respectively, were unsuccessful, probably due to the limitation of our laser system (laser pulse width 8−10 ns), as such processes are expected to be faster than the nanosecond time scale.

All the complexes were tested for their gelation properties in various organic solvents by the "stable-to-inversion-of-test-tube" method, and they were found to form stable yellow translucent metallogels at critical gelation concentrations of less than 10 mg/mL in benzene. To study the morphologies of the benzene xerogels formed by the complexes, scanning electron microscopy (SEM) images were recorded. As shown in Figure 4, all the complexes formed a network of fibrous structures in their xerogels. The fibers are on the micrometer scale, comparable to the situation observed in typical metallogels and organogels.[3g,4b,6,7] Upon increasing the temperature above their sol−gel transition temperature (T_{gel}), metallogels of **1** and **3** in benzene formed orange sols, while that of **2** formed a yellowish-orange sol. The photographs of the metallogels and their corresponding sol forms are shown in Figure 5a,b. Interestingly, the metallogel of **1** showed drastic luminescence enhancement during the phase transition from the gel form to the sol form (Figure 5c,d), which could rarely be found in other typical thermotropic organogels and metallogels. This is because, in general, it is only during gel formation that luminescence enhancement arising from the rigidification of the molecules which slows down the non-radiative deactivation processes would occur, while the sol form which usually occurs at elevated temperature would be non-emissive due to the more efficient non-radiative decay of the excited-state molecules at high temperatures.[3g,6c,h−j,7d] To the best of our knowledge, there was only one report on a class of trinuclear Au(I) pyrazolate metallacyclic complexes that showed luminescence diminishment upon a sol-to-gel phase transition at 298 K.[7b]

Owing to the unusual behavior of **1** during the gel-to-sol phase transition, temperature-dependent emission studies in the gel state ([**1**] = 5.6×10^{-3} M) were performed. Upon excitation at the isosbestic wavelength of 450 nm of the UV−vis spectral traces (Figure 6a), a vibronic-structured emission band at 550 nm was observed at 283 K. Upon increasing the temperature from 283 to 323 K, a low-energy emission band at 650 nm grew dramatically in intensity and reached a maximum intensity at 333 K, which is close to the sol−gel transition temperature.[11] As the temperature is further increased above 333 K, the emission intensity starts to decrease due to a significant increase in the rate of non-radiative decay at high temperature. The emission spectral changes as a function of temperature are shown in Figure 6b. Theoretically, the overall emission intensity is exponentially related to the reciprocal of temperature, resulting from the temperature-dependent deactivation processes.[12] A plot of $\ln(I/I_o)$ monitored at 650 nm against the reciprocal of temperature was obtained (Figure 6c), indicating an increase in the emission intensity with an increase in temperature from 283 to 323 K, reaching a maximum at the sol−gel transition temperature. The high-energy vibronic-structured emission band that predominates at 283 K with vibrational progressional spacings of *ca.* 1300 cm^{-1} is assigned to a metal-perturbed ^{3}IL [$\pi \rightarrow \pi^*$(bzimpy)] state.[9] On the basis of the temperature-dependent emission study of **1** in dilute benzene solution, the new structureless emission at 650 nm is attributed to excimeric emission, which is derived from the enhanced metal−metal and $\pi-\pi$ interactions in the excited state. As an excimeric emission band appeared at high temperature during the gel-to-sol phase transition of complex **1**, complex **2** was synthesized to explore the effect of planarization between the bzimpy and phenylethynyl ligands on the formation of aggregate species upon incorporation of a methyl substituent at the *ortho* position of the ethynyl group. Excitation of a benzene gel of **2** at 450 nm (isosbestic wavelength in the variable-temperature UV−vis spectral traces) shows a drop in monomeric emission intensity upon increasing the temperature (Figure 7). The reason for the different behavior, when compared to that of **1**, is the lack of aggregate formation for non-planar molecules in benzene, resulting from the steric repulsion between the hydrogen atoms at the 4,4′-positions of the two benzimidazolyl groups (as denoted in Scheme 1) and the methyl group *ortho* to the ethynyl unit of the aryl ring,[13] although an increase in non-radiative decay of the excited molecules at high temperature could not be excluded. In contrast, complex **3** shows a luminescence enhancement during the gel-to-sol phase transition (Figure S1, Supporting Information) similar to that observed in **1**, confirming that the lack of such enhancement in **2** is not ascribed to the introduction of the electron-rich methyl substituent. We believe

(11) Since an increase in temperature would lead to a decrease in dissolved oxygen content in solution and thereby the solution might become more strongly luminescent due to a reduced quenching effect of dioxygen, a control experiment was performed using degassed benzene under an inert atmosphere. The close resemblance of the changes in the emission intensity as a function of temperature to that measured in non-degassed benzene gel indicates that the luminescence enhancement upon increasing the temperature is not due to the removal of dissolved oxygen content in the sol state.

(12) (a) Suárez, S.; Imbert, D.; Gumy, F.; Piguet, C.; Bünzli, J.-C. G. *Chem. Mater.* **2004**, *16*, 3257. (b) Kleinerman, M.; Choi, S.-I. *J. Chem. Phys.* **1968**, *49*, 3901.

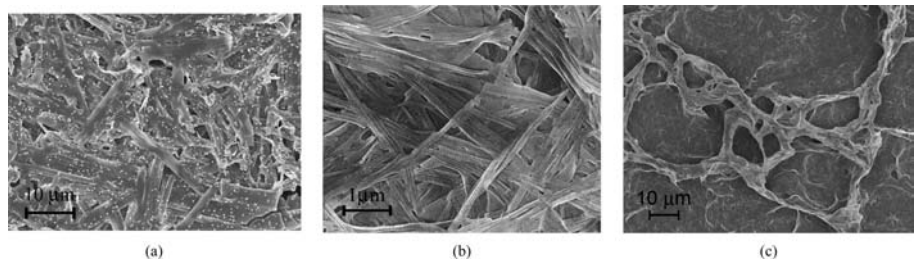

Figure 4. SEM images of the benzene metallogels of (a) **1**, (b) **2**, and (c) **3**.

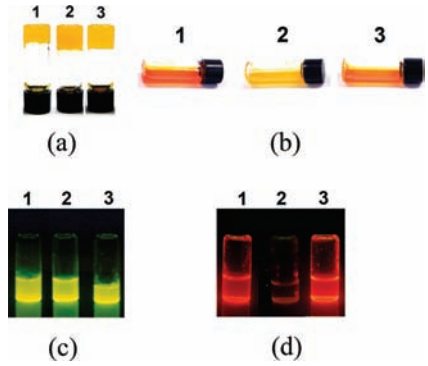

Figure 5. Photographs of **1**, **2**, and **3** in (a) the gel forms at room temperature, (b) the sol forms at elevated temperature, (c) the gel forms under UV illumination, and (d) the sol forms under UV illumination.

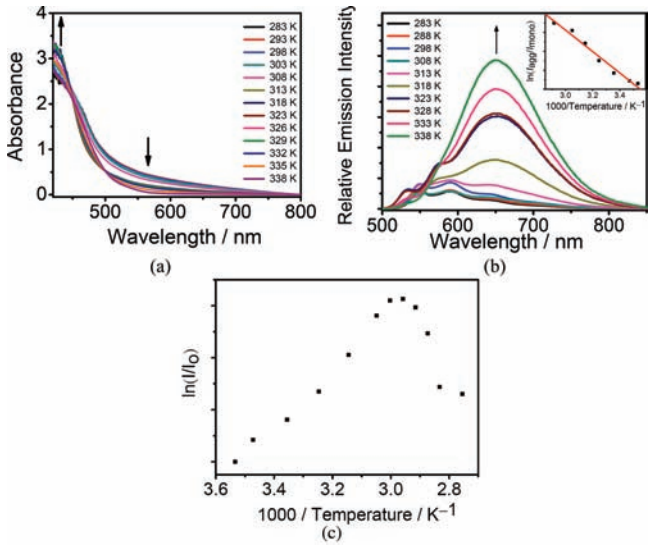

Figure 6. (a) UV−vis absorption spectra of metallogel **1** upon increasing the temperature from 283 to 338 K. (b) Corrected emission spectra of the benzene gel of **1** at various temperatures in the range 283−333 K (total [Pt] concentration = 5.6×10^{-3} M). Inset: Corresponding Stevens−Ban plot of $\ln(I_{agg}/I_{mono})$ vs $1/T$ (where I_{agg} and I_{mono} are the emission intensities at 650 and 550 nm at the corresponding temperatures respectively). (c) Plot of $\ln(I/I_o)$ vs the reciprocal of temperature (where I is the emission intensity at 650 nm at a given temperature and I_o is the emission intensity at 650 nm at 283 K).

that one of the reasons for the luminescence enhancement during the gel-to-sol phase transition observed in **1** and **3** is associated with the restricted molecular geometry and packing imparted by the formation of fibrous networks in the gel phase. It is likely that the molecules cannot move or rotate freely to undergo intermolecular aggregation and oligomerization processes via self-association.[6h] However, upon increasing the temperature, an increase in the degrees of freedom and motion of the

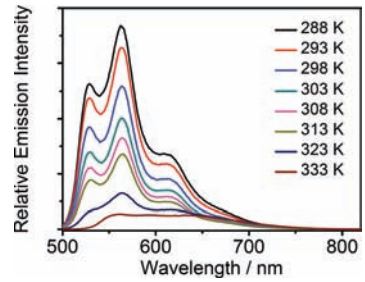

Figure 7. Corrected emission spectra of the metallogel **2** in benzene at various temperatures in the range 288−333 K (concentration = 5.6×10^{-3} M).

molecules could result in a higher chance to form molecular assemblies and aggregates, resulting in an increase in the excimer population. On the other hand, the presence of a sterically encumbered *ortho* substituent in **2** does not allow such an assembly to occur. In addition, the luminescence quantum yield of the excimeric excited state is likely to be much higher than that of the ^{3}IL excited state, leading to a more strongly luminescent sol form than the gel form with an identical number of photons absorbed.

A detailed quantitative treatment of the temperature-dependent emission spectral changes of metallogel **1** in benzene has also been performed. Interestingly, the temperature-dependent emission study of the metallogel **1** in the high concentration regime ($\sim 10^{-2}-10^{-3}$ mol dm^{-3}) in the temperature range of 283−333 K yielded a slope that turned negative in the Stevens−Ban plot, as compared to that in dilute benzene solution. This suggests that the system changes to the low-temperature limit in the gel phase. From the slope, the activation energy for the excimer formation of 47.03 ± 3.28 kJ mol^{-1} was obtained (Figure 6b, inset).[10] The identity of the aggregate (mostly in the form of dimers) has also been supported by positive-ion FAB mass spectral studies of metallogel **1**, which show, apart from the presence of the monomeric species ($[M - PF_6]^+$), the presence of the dimeric species ($[M_2 - PF_6]^+$). The expanded ion cluster of the dimeric species in the positive-ion FAB mass spectrum and its corresponding simulated isotope pattern are shown in Figure 8. Similar observations of dimeric species by mass

(13) A molecular model in which the plane of the aryl ring of the alkynyl ligand is coplanar to the [Pt(bzimpy)] plane has been built by the program GaussView, which shows that the *ortho* methyl protons on the arylalkynyl ligand in **2** are relatively close to the hydrogen atoms at the 4,4′-positions of the bzimpy ligand (separation distance = 1.79 Å), as compared to the *ortho* protons on the phenylalkynyl ligand in **1** (separation distance = 2.42 Å). It is interesting to note that, even with **1**, an interplanar angle between the planes of the arylalkynyl and [Pt(bzimpy)] of larger than 30° has been observed in ref 9. A related work involving the use of steric effects to demonstrate the excimeric nature of an emission has been reported: Mdleleni, M. M.; Bridgewater, J. S.; Watts, R. J.; Ford, P. C. *Inorg. Chem.* **1995**, *34*, 2334.

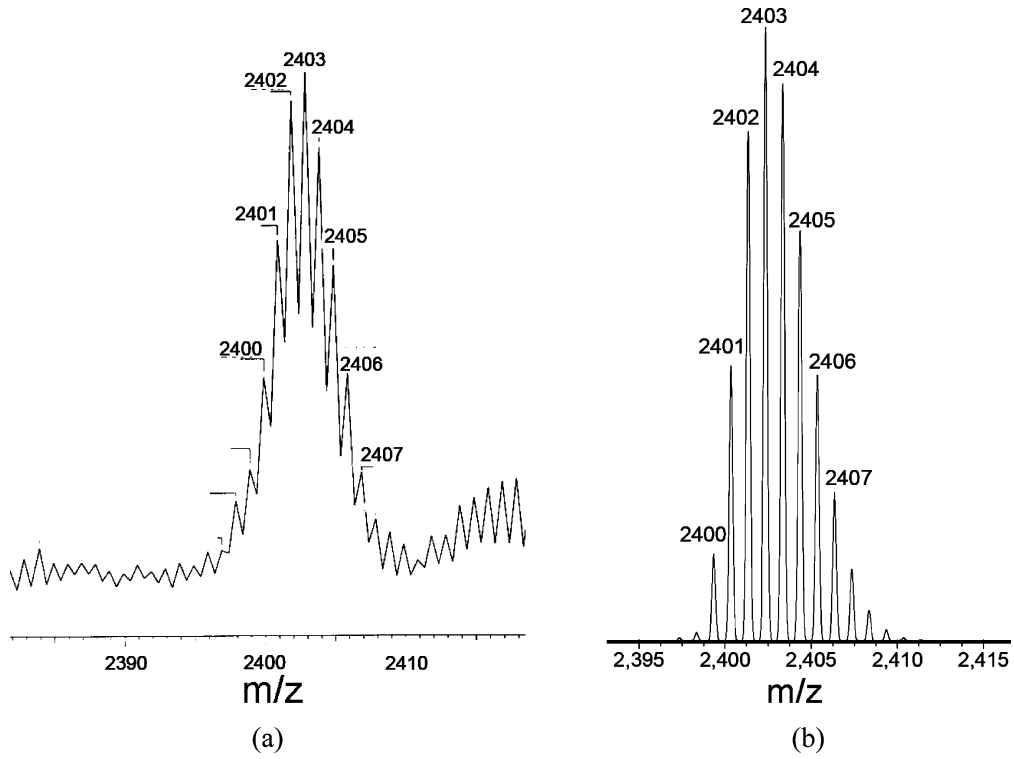

Figure 8. (a) Positive-ion FAB mass spectrum of metallogel **1** in benzene, showing the expanded ion cluster corresponding to the dimeric species ($[M_2 - PF_6]^+$) in gel form, and (b) its corresponding simulated isotope pattern.

Table 2. Variable-Temperature Lifetime Data Monitored at Different Wavelengths of Metallogel **1** in Benzene

	lifetime τ_o/μs				
T/K	540 nm	550 nm	715 nm	725 nm	735 nm
288	0.48	0.52	0.25	0.27	0.23
298	0.40	0.44	0.22	0.22	0.22
308	0.40	0.40	0.22	0.19	0.22
313	0.37	0.38	0.21	0.20	0.21
318	0.32	0.33	0.21	0.21	0.18
328	0.19	0.22	0.17	0.17	0.16
338	0.13	0.14	0.13	0.13	0.11
348	0.10	0.11	0.09	0.10	0.09

spectrometry in other systems with weak metal−metal interactions have also been recently reported.[14] A time-dependent emission experiment on the metallogel **1** was also performed. After the gel-to-sol phase transition was reached, the low-energy emission band dropped in intensity with concomitant growth of the high-energy vibronic-structured emission band with time (Figure S2, Supporting Information). The inset of Figure S2 shows the changes in the emission band intensities of the high- and low-energy bands at 540 and 735 nm with time, indicating that the drop in the excimeric emission intensity parallels the growth of the monomeric emission intensity with time. Such changes with time may be considered as an alternative representation of the interconversion between the excimeric and the monomeric emissive states with temperature. Variable-temperature lifetime measurements were also performed ($[\mathbf{1}] = 5.9 \times 10^{-3}$ M). At $T = 288$ K, the lifetimes monitored at 540 and 735 nm were 0.48 and 0.23 μs, respectively, corresponding to the lifetimes of the monomeric and excimeric excited states. The lifetimes monitored at different wavelengths are summarized in Table 2. Upon increasing the temperature, both lifetimes were found to decrease due to an increase in the non-radiative decay rate constant. As the temperature increases above 318 K, the lifetime monitored at 540 and 735 nm is mainly dominated by that of the low-energy excimeric emission component, similar to the observation in the variable-temperature emission study.

Conclusion

As the rate of non-radiative decay would usually increase with increasing temperature, an increase in luminescence intensities upon an increase in temperature and during the gel-to-sol phase transition at elevated temperatures is rarely observed. In this paper, we have demonstrated a unique example of metallogels that shows an unusual luminescence enhancement during the gel-to-sol phase transition upon increasing the temperature. On the basis of the Birks kinetic scheme, the binding enthalpy (ΔH), binding entropy (ΔS), and Gibbs free energy change (ΔG) of the excimer formation were determined to be -43.77 kJ mol^{-1}, -44.14 J mol^{-1} K^{-1}, and -30.62 kJ mol^{-1}, respectively. Concentration-dependent and variable-temperature luminescence studies revealed that the unique luminescence enhancement is due to the removal of restricted molecular geometry that favors the formation of aggregate species in the sol form at high temperature. This property may lead to the design of promising potential colorimetric and

(14) Krishantha, D. M. M.; Gamage, C. S. P.; Schelly, Z. A.; Dias, H. V. R. *Inorg. Chem.* **2008**, *47*, 7065.

(15) (a) Huang, M. H.; Soyez, H. M.; Dunn, B. S.; Zink, J. I.; Sellinger, A.; Brinker, C. J. *J. Sol-Gel. Sci. Technol.* **2008**, *47*, 300. (b) Angelos, S.; Johansson, E.; Stoddart, J. F.; Zink, J. I. *Adv. Funct. Mater.* **2007**, *17*, 2261. (c) Huang, M. H.; Dunn, B. S.; Zink, J. I. *J. Am. Chem. Soc.* **2000**, *122*, 3739.

luminescence reporters for microenvironmental changes, as well as potential multifunctional metallogels and smart materials.[7e,15]

Experimental Section

Materials and Reagents. Phenylacetylene and (4-methylphenyl)acetylene were obtained from Aldrich Chemical Co. (2-Methylphenyl)acetylene was purchased from Maybridge Chemical Co. Ltd. The chloroplatinum(II) bzimpy precursor was synthesized as described previously.[9] All solvents were purified and distilled using standard procedures before use. All other reagents were of analytical grade and were used as received.

Synthesis. Synthesis of 1. To a degassed solution of the chloroplatinum(II) precursor[9] (200 mg, 0.17 mmol) in CH_2Cl_2 (50 mL) were added phenylacetylene (0.06 g, 0.58 mmol), a catalytic amount of CuI (2 mg, 5%), and NEt_3 (1 mL). The resultant solution was stirred at room temperature under N_2 overnight. After removal of solvent, the residue was purified by column chromatography on silica gel using dichloromethane−acetone (6:1 v/v) as eluent. Subsequent recrystallization by diffusion of diethyl ether vapor into a dichloromethane solution of the product gave **1** as a yellow solid. Yield: 164 mg (78%). ^{1}H NMR (400 MHz, CD_3CN, 333 K, relative to Me_4Si, δ/ppm): 0.96 (m, 9H, -CH_3), 1.47 (m, 54H, -CH_2-), 1.86 (m, 6H, -CH_2-), 3.91 (t, 2H, J = 6.7 Hz, -OCH_2-), 4.31 (t, 4H, J = 7.8 Hz, -NCH_2-), 7.23 (m, 4H, pyridine and benzimidazole), 7.28 (t, 2H, J = 7.9 Hz, benzimidazole), 7.57 (m, 4H, benzimidazole and -Ph), 7.36 (m, 3H, -Ph), 8.45 (d, 2H, J = 7.9 Hz, benzimidazole). IR (Nujol, ν/cm^{-1}): 2114 (w), ν(C≡C); 753 (s), ν(P−F). Positive FAB-MS: m/z 1128 $[M - PF_6]^+$. Anal. Calcd for $C_{63}H_{90}F_6N_5OPPt\cdot H_2O$: C, 58.59; H, 7.18; N, 5.42. Found: C, 58.42; H, 6.92; N, 5.37.

Synthesis of 2. The procedure was similar to that for complex **1**, except (2-methylphenyl)acetylene (40 mg, 0.33 mmol) was used in place of phenylacetylene. Yield: 176 mg (57%). ^{1}H NMR (400 MHz, $CDCl_3$, 298 K, relative to Me_4Si, δ/ppm): 0.92 (m, 9H, -CH_3), 1.47 (m, 54H, -CH_2-), 1.84 (m, 6H, -CH_2-), 2.54 (s, 3H, -CH_3 of phenylacetylene), 4.01 (t, J = 6.9 Hz, 2H, -OCH_2-), 4.46 (t, J = 7.7 Hz, 4H, -NCH_2-), 7.00 (d, J = 8.5 Hz, 2H, benzimidazole), 7.38 (m, 10H, benzimidazole, pyridine and -C_6H_4-), 8.26 (d, J = 8.2 Hz, 2H, benzimidazole). IR (Nujol, ν/cm^{-1}): 2115 (w), ν(C≡C); 749 (s), ν(P−F). Positive FAB-MS: m/z 1143 $[M - PF_6]^+$. Anal. Calcd for $C_{63}H_{90}F_6N_5OPPt$: C, 59.70; H, 7.20; N, 5.44. Found: C, 59.89; H, 7.26; N, 5.52.

Synthesis of 3. The procedure was similar to that for complex **1**, except (4-methylphenyl)acetylene (40 mg, 0.33 mmol) was used in place of phenylacetylene. Yield: 170 mg (63%). ^{1}H NMR (400 MHz, $CDCl_3$, 298 K, relative to Me_4Si, δ/ppm): 0.94 (m, 9H, -CH_3), 1.55 (m, 54H, -CH_2-), 1.91 (m, 6H, -CH_2-), 2.66 (s, 3H, -CH_3 of phenylacetylene), 4.16 (t, J = 6.9 Hz, 2H, -OCH_2-), 4.60 (t, J = 6.9 Hz, 4H, -NCH_2-), 7.38 (s+m, 7H, benzimidazole, pyridine, and -C_6H_4-), 7.55 (m, 5H, benzimidazole and -C_6H_4-), 8.54 (d, J = 7.9 Hz, 2H, benzimidazole). IR (Nujol, ν/cm^{-1}): 2114 (w), ν(C≡C); 751 (s), ν(P−F). Positive FAB-MS: m/z 1143 $[M - PF_6]^+$. Anal. Calcd for $C_{63}H_{90}F_6N_5OPPt\cdot 0.5CH_2Cl_2$: C, 57.95; H, 6.97; N, 5.32. Found: C, 57.65; H, 7.14; N, 5.49.

Physical Measurements and Instrumentation. ^{1}H NMR spectra were recorded on a Bruker AVANCE 400 (400 MHz) Fourier-transform NMR spectrometer with chemical shifts reported relative to tetramethylsilane, $(CH_3)_4Si$. Positive-ion FAB mass spectra were recorded on a Finnigan MAT95 mass spectrometer. To obtain the positive-ion FAB mass spectrum of the gel sample, the benzene gel was mixed with the matrix, *m*-nitrobenzyl alcohol (NBA), so that the gel state is not easily destroyed by the high-energy particle beam. The gel/matrix mixture was coated onto the FAB probe and then injected into the positive-ion FAB ionization chamber, in which the monomeric and dimeric molecules were bombarded by high-energy cesium ions to form cationic species. The resultant cationic species were detected. IR spectra were obtained as Nujol mulls on KBr disks on a Bio-Rad FTS-7 Fourier transform infrared spectrophotometer (4000−400 cm^{-1}). Elemental analyses of the newly synthesized complexes were preformed on a Flash EA 1112 elemental analyzer at the Institute of Chemistry, Chinese Academy of Sciences.

The electronic absorption spectra were obtained using a Hewlett-Packard 8452A diode array spectrophotometer. The concentrations of solution samples for electronic absorption measurements were typically in the range from 2×10^{-3} to 2×10^{-5} mol dm^{-3}. Steady-state excitation and emission spectra at room temperature and at 77 K were recorded on a Spex Fluorolog-3 model FL3-211 fluorescence spectrofluorometer equipped with a R2658P PMT detector. Solid-state photophysical studies were carried out with solid samples contained in a quartz tube inside a quartz-walled Dewar flask. Measurements of the butyronitrile glass or solid-state sample at 77 K were similarly conducted with liquid nitrogen filled into the optical Dewar flask. The concentrations of complex solutions in butyronitrile for glass emission measurements were usually on the order of 10^{-6} mol dm^{-3}. All solutions for photophysical studies were degassed on a high-vacuum line in a two-compartment cell consisting of a 10-mL Pyrex bulb and a 1-cm or 4-mm path length quartz cuvette and sealed from the atmosphere by a Bibby Rotaflo HP6 Teflon stopper. The solutions were rigorously degassed with at least four successive freeze−pump−thaw cycles. Emission lifetime measurements were performed using a conventional laser system. The excitation source used was the 355-nm output (third harmonic) of a Spectra-Physics Quanta-Ray Q-switched GCR-150-10 pulsed Nd:YAG laser. Luminescence decay signals were detected by a Hamamatsu R928 PMT, recorded on a Tektronix model TDS-620A (500 MHz, 2 GS/s) digital oscilloscope, and analyzed using a program for exponential fits. Time-resolved emission spectra were recorded on an Oriel Instruments intensified charge-coupled device (ICCD) detector (model DH520) and were analyzed using the InstaSpec V software. The excitation source is the same laser system as that used for lifetime measurement. The emission signal was collected by an optical fiber and dispersed onto the CCD detector with an Oriel MultiSpec 115 imaging spectrograph (model 77480). A Stanford Research Systems (SRS) delay generator (model DG 535) was used to produce the transistor−transistor logic (TTL) pulse needed to operate the intensifier gating electronics in the detector head. The external trigger input of the delay generator was connected to the laser's prepulse trigger output. The delay generator was controlled via an IBM AT APIB (IEEE 488) card interfaced with an IBM-compatible Pentium personal computer to allow the InstaSpec V software to send commands to control the width and delay of the TTL pulse. The system was operated at −15 °C by the single-stage system in order to reduce the dark current signal.

Variable-temperature UV−vis absorption and emission spectra were obtained using a Varian Cary 50 UV−vis spectrophotometer and a Spex Fluorolog-3 model FL3-211 fluorescence spectrofluorometer equipped with a R2658P PMT detector, respectively. The variable-temperature emission lifetime measurements were performed using the same laser system as described above. These measurements were recorded with a single-cell Peltier thermostat to control the working temperature in the range of 288−373 K. The gel samples were measured in a 1-mm path length quartz cuvette and a 4-mm path length quartz cuvette for UV−vis absorption and emission measurements, respectively. The dilute solution sample was measured in a 1-cm path length quartz cuvette for UV−vis absorption and emission measurements.

Electron Microscopy. Scanning electron microscopy (SEM) experiments were performed on a Leo 1530 FEG instrument operating at 4.0−6.0 kV. The SEM samples were prepared by dropping dilute gels onto a silicon wafer. Slow evaporation of solvents in air for 10 min led to xerogels. All the samples for SEM experiments were sputtered with gold thin film.

Determination of Thermodynamic and Kinetic Parameters of Monomer−Excimer Equilibrium. The ratio of the excimeric to monomeric emission intensities could be described by eq 1, based on the Birks scheme,[10]

$$\frac{I_{agg}}{I_{mono}} = \frac{k_{fD}k_{DM}[M]}{k_{fM}(k_D + k_{MD})} \quad (1)$$

where k_{fD} and k_{fM} are the excimer and monomer radiative rate constants, respectively, while k_{DM} and k_{MD} are the excimer formation and dissociation rate constants, respectively. k_D is the excimer decay rate constant.

For the system under the high-temperature limit, k_{MD} is much larger than k_D, and eq 1 is simplified to eq 2.

$$\frac{I_{agg}}{I_{mono}} = \frac{k_{fD}k_{DM}[M]}{k_{fM}k_{MD}} \quad (2)$$

Since k_{fD} and k_{fM} are temperature-independent, a plot of $\ln(I_{agg}/I_{mono})$ against $1/T$ (Stevens−Ban plot) yields a straight line with a positive slope, which is equal to $-\Delta H/R$ (where ΔH is the enthalpy for the excimer formation). Also, the y-intercept is equal to $-\ln(k_{fM}/k_{fD}[M]) + (\Delta S/R)$, where ΔS is the excimer binding entropy. To determine the ratio of k_{fM}/k_{fD}, a graph of I_{agg} against I_{mono} at concentration = [M] with a negative slope was plotted, and its slope is equal to $-k_{fD}/k_{fM}$. The binding entropy can be calculated on the basis of this relationship.[10d]

For the system under low-temperature limit, k_{MD} is much smaller than k_D, and eq 1 is simplified to eq 3.

$$\frac{I_{agg}}{I_{mono}} = \frac{k_{fD}k_{DM}[M]}{k_{fM}k_D} \quad (3)$$

The Stevens−Ban plot under this limit gives a straight line with a negative slope, which is equal to $-E_a/R$ (where E_a is the activation energy for the excimer formation).

Acknowledgment. V.W.-W.Y. acknowledges support from The University of Hong Kong under the Distinguished Research Achievement Award Scheme and the URC Strategic Research Theme on Molecular Materials. This work has been supported by the RGC Central Allocation Vote (CAV) Grant (HKU 2/05C), and the National Natural Science Foundation of China and the Research Grants Council of Hong Kong Joint Research Scheme (NSFC-RGC Project No. N_HKU 737/06). A.Y.-Y.T. acknowledges the receipt of a postgraduate studentship, administered by The University of Hong Kong. We also thank Mr. Frankie Yu-Fee Chan at the Electron Microscope Unit of The University of Hong Kong for helpful technical assistance.

Supporting Information Available: Corrected emission spectra of the metallogel **3** in benzene at 298 and 343 K; time-dependent emission spectra at 298 K after the gel-to-sol phase transition. This material is available free of charge via the Internet at http://pubs.acs.org.

JA900895X